Electric double-layer interactions in a wedge geometry: Change in contact angle for drops and bubbles

Siddhartha Das* and Sushanta K. Mitra
Department of Mechanical Engineering, University of Alberta, Edmonton, Alberta, Canada T6G 2G8
(Received 27 June 2013; revised manuscript received 1 September 2013; published 26 September 2013)

In this paper, we provide a theory to pinpoint the role of electric double layer (EDL) interactions in governing the contact angle of an electrolyte drop on a charged solid in air or a bubble on a charged surface within an electrolyte solution. The EDL interactions are analytically solved by representing the three phase contact line as a wedge edge, with the wedge being formed by the solid-liquid and the air-liquid interfaces, and calculating the corresponding Maxwell stresses. We demonstrate that the EDL effects induce an "electrowetting-like" behavior, resulting in a lowering of the contact angle. As a specific example, we use this model to analyze the effect of added salt on preformed surface nanobubbles, and find, in contrast to what has been reported earlier, that even for most moderate conditions, added salt may have remarkable effect in altering the contact angle in preformed surface nanobubbles.

DOI: 10.1103/PhysRevE.88.033021 PACS number(s): 47.55.db

I. INTRODUCTION

Determination of the contact angle of a drop on a solid, application of external means to alter this contact angle, and understanding the resulting contact line dynamics during this alteration process form the founding basics of the subjects of *wetting* and *capillarity* [1–7]. While a drop of a given liquid demonstrates a unique value of the contact angle on a given partially wetting solid in a given surrounding, practical and technological requirements have motivated development of methods that may enforce a change in this intrinsic contact angle value. For example, periodic micronanostructures have been engineered on the solid to ensure an enhancement in the contact angle value by enforcing the drop to attain a *Fakir* or a *Cassie-Baxter* state [8–12]. Similarly, one of the most popular techniques to decrease this contact angle has been the application of an external electric field—this is the well-known science of *electrowetting*, where the electrostatic tension induced by the electric field augments the wetting behavior resulting in a decrease in the contact angle [13,14].

Electrowetting problems form a small subset of a bigger problem set of *electrocapillarity*, which encompasses all the problems dictated by the interplay of the capillarity and electric effects. These electric effects can be static in nature, where electrostatic forces may lead to a change in contact angle [13–21], or may be dynamic in nature where the resulting electric current can substantially affect the capillary dynamics [22,23]. For the static problem, per unit area electrostatic wetting tension (having the units of energy per unit area) W_{el} scales as CV^2 (where C is the capacitance and V is the voltage) and the ratio CV^2/γ (where γ is the liquid-vapor surface tension) dictates the contribution of the electrostatic effects in modifying the contact angle. For an electrowetting problem, these parameters (C and V) can be easily determined from the system definition [13,14]. Such electrowetting behavior may be important even when there is no external voltage. This typically occurs for the case of the wetting of an electrolyte drop on a charged surface in air or the formation of a bubble on a charged solid in the presence of a background electrolyte solution. In such a situation, an electric double layer (EDL) [24] develops at the interface of the charged solid and the electrolyte solution, and this V is the EDL electrostatic potential (that varies within the drop) and the capacitance is the dielectric capacitance of the EDL [15]. There are plenty of examples in recent literature, where such EDL-mediated electrical effects have been influential in affecting different dynamic and static capillary problems [15,16,22,23,25,26]. However, in all those studies, the EDL electrostatics have been simplified by considering only a one-dimensional EDL, without pinpointing the consequences of the wedge geometry that invariably appears at the three phase contact line (TPCL) of the drop [17–21].

In this paper, we provide an analysis that represents the TPCL as a wedge, calculate the EDL electrostatic distribution in such a wedge geometry (following the method of Dörr and Hardt [27]), and use this calculation to obtain the resulting Maxwell stress and the corresponding change in the drop or bubble contact angle. The magnitude of the change in the contact angle depends on the values of parameters such as *p*H, surface charge density, electrolyte ion concentration, etc.—we provide results for substrates such as bare silica and OTS [(octadecyltrichlorosilane)-silicon], for which there exist well-known relationships between the charge density, buffer *p*H, and the EDL thickness [15,28,29]. Our work is distinctly different from that of Dörr and Hardt [27] in the sense that they obtain the EDL electrostatics at the TPCL, and we use this analysis to compute the Maxwell stress and the resulting alteration of the drop or bubble contact angle. The present model is derived on the basis of several simplifying assumptions. First, we assume that only the solid-liquid interface of the wedge is charged, whereas the air-water interface is uncharged. Such an assumption has been well reported in the literature, [17,18,27,30–32], although there are also studies that conjecture the presence of a finite charge at the air-water interface [33–36]. Also these physical situations are represented with the boundary conditions of a specified charge density σ (or the

*sdas1@ualberta.ca

corresponding normal electric field) at the solid-liquid interface, and zero charge (hence zero normal electric field) at the air-water interface. For substrates such as bare silica and OTS-silicon, for which we provide our results, this charge density gets fixed by parameters such as bulk pH and bulk electrolyte ion concentration [15,28,29]. The second assumption concerns the value of this charge density at the solid-water interface. We assume that the corresponding surface potential $\sim\sigma\lambda/\epsilon_0\epsilon_r$ (where λ is the EDL thickness, ϵ_0 is the permittivity of free space, and ϵ_r is the relative permittivity of water) is substantially small so that we can employ Debye-Hückel linearization [24] to solve the EDL potential (see later). Finally, we operate at an ionic concentration such that the corresponding EDL thickness λ is substantially smaller than the dimensions of the drop or the bubble—this assumption is necessary for representing the region around the TPCL as a wedge.

The central result of the study points to a substantially large decrease in the contact angle of the drop or bubble for both bare silica and OTS-silicon substrates as a function of buffer pH, bulk ionic concentration, and the initial EDL-independent values of the contact angle. The current analysis, although applicable for predicting contact angles of bubbles or drops with EDL effects, was motivated to understand the role of added salt in changing the morphologies of *preformed* surface nanobubbles [37–57]. We had earlier demonstrated, through a scaling analysis, that added salt can have substantial impact on the nanobubble morphology only for very alkaline buffer pH [15]. On the contrary, in the present study we show that proper accounting for the EDL electrostatics at the wedge TPCL meant that we can substantially improve our predictions, and observe substantial variation in the nanobubble contact angle (formed on the OTS-silicon surface) even for an extremely moderate buffer pH.

II. THEORY

A. Contact angle with the EDL effects

Figure 1(a) shows the schematic of a bubble on a charged surface inside an electrolyte solution and an electrolyte drop in air on a charged surface represented as a spherical cap. These are the two cases where the EDL (triggered at the interface of the charged solid and the electrolyte) will affect the contact angle. The TPCL of the drop or the bubble can be approximated as a wedge edge, with the two sides of the wedge being the solid-liquid and air-liquid interfaces [see Fig. 1(b)]. Such wedge-edge approximation of the TPCL has been a popular approach used to study the relevant electrostatics at the TPCL [17–21]. There are no ions (or EDL) inside the bubble or the air (for the case of the drop), and the EDL is confined only at the liquid side [see Fig. 1(b)]. We assume that the presence of the EDL provides an additional energy (per unit length) of W_{el}. The effect of the EDL on the contact angle can be obtained from the free energy change occurring on account of the air-liquid interface being displaced by a distance dx towards the liquid side [in Fig. 1(b)]. Such a displacement implies the creation of an additional solid-air interface and an equivalent destruction of the solid-liquid interface. Accordingly, there will be an increase in surface energy (per unit length) of $(\gamma_{SV} + \gamma_{LV}\cos\theta)dx$ and a decrease in surface energy

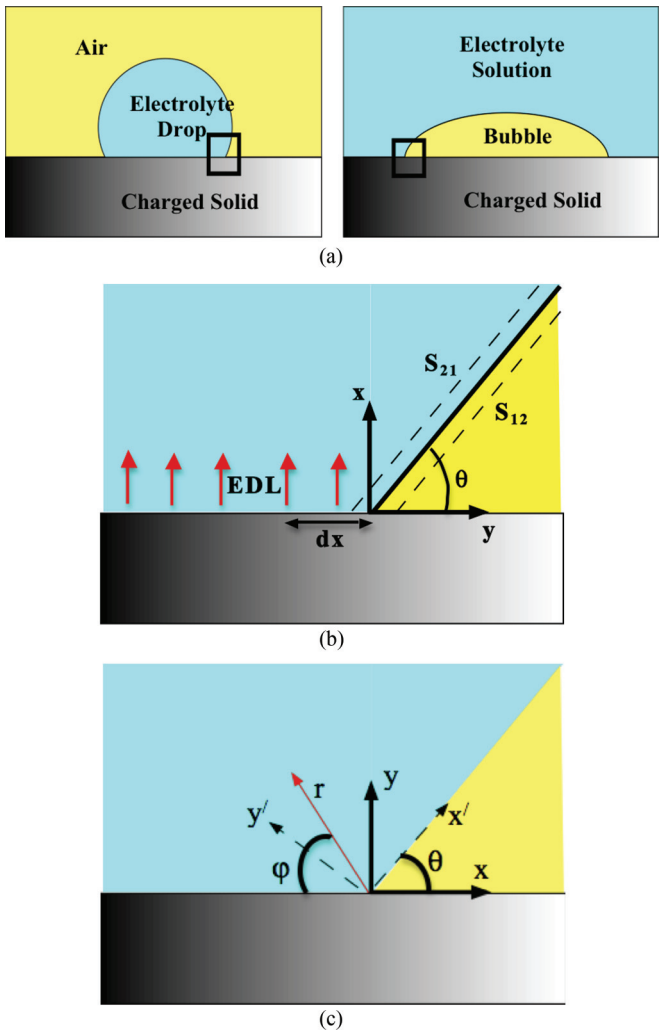

FIG. 1. (Color online) (a) Left: schematic of the electrolyte drop placed in air. Right: schematic of the bubble inside an electrolyte drop. (b) Magnified view of the TPCL [indicated by a black hollow rectangle in (a)]. This magnified view defines the different parameters, e.g., contact angle, the planes S_{12} and S_{21} in the air and the liquid sides, the EDL at the the solid-liquid and liquid-vapor interfaces, and the $(x$-$y)$ coordinate axes. Here the wedge is considered to be filled with liquid only, and hence the wedge angle is $\pi - \theta$. We also show the distance dx moved by the TPCL. (c) Definition of the axes x'-y' and the r-φ coordinate system.

by $\gamma_{SL}dx$. Additionally, the destruction of the solid-liquid interface would mean an equivalent destruction of the EDL, which will lead to a further decrease in the energy (per unit length) by $W_{el}(\theta)dx$. Here γ_{ij}'s are the interfacial tensions between phases i and j (L, S, and V stand for liquid, solid, and vapor or air), θ is the equilibrium contact angle (with finite accounting of the EDL interaction effects), and $W_{el}(\theta)$ is the EDL-induced electrostatic wetting tension (per unit length), which is a function of the contact angle θ. Hence at equilibrium, we can write

$$dE = [\gamma_{SV} - \gamma_{SL} + \gamma_{LV}\cos\theta - W_{el}(\theta)]\,dx = 0$$
$$\Rightarrow \cos\theta = \cos\theta_0 + \frac{W_{el}(\theta)}{\gamma_{LV}}, \quad (1)$$

where $\theta_0 = \cos^{-1}(\frac{\gamma_{SL}-\gamma_{SV}}{\gamma_{LV}})$ is the Young's angle. We shall get the drop or the bubble equilibrium contact angle by solving for θ iteratively from Eq. (1).

B. Calculation of the EDL-induced electrostatic wetting tension

To determine the influence of the EDL electrostatic wetting tension on the contact angle, we need to determine $W_{el}(\theta)$. Following [17–21,56], we can express W_{el} as [assuming that there is no charge or electrostatic field inside the bubble or the air (for the case of the drop)]

$$W_{el} = -\mathbf{e}_x \int_{S_{21}} \hat{\mathbf{T}} \cdot (-\mathbf{n}) dS = \mathbf{e}_x \int_{S_{21}} \left[-\Pi \hat{\mathbf{I}} + \epsilon_0 \epsilon_w \left(\mathbf{E}\mathbf{E} - \frac{1}{2} E^2 \mathbf{I} \right) \right] \cdot (\mathbf{n}) dS, \quad (2)$$

where $\hat{\mathbf{T}}$ is the Maxwell stress tensor, expressed as $\hat{\mathbf{T}} = [-\Pi \hat{\mathbf{I}} + \epsilon_0 \epsilon_w (\mathbf{E}\mathbf{E} - \frac{1}{2} E^2 \mathbf{I})]$ (Π is the osmotic pressure, $\mathbf{E}$ is the electric field vector, E is the magnitude of the electric field, ϵ_0 is the permittivity of free space, ϵ_w is the relative permittivity of water, $\hat{\mathbf{I}}$ is the identity tensor, $\mathbf{e}_x$ is the unit normal vector along the x direction, and $\mathbf{n}$ is the outward unit normal vector to the air-water interface). We can reduce the above equation using the identities $\hat{\mathbf{I}} \cdot \mathbf{n} = \mathbf{n}$, $(\mathbf{E}\mathbf{E}) \cdot \mathbf{n} = (\mathbf{n} \cdot \mathbf{E})\mathbf{E}$, $\mathbf{n} = -\sin\theta \mathbf{e}_x + \cos\theta \mathbf{e}_y$ ($\mathbf{e}_y$ is the unit normal vector along the y direction), and $\mathbf{E} = E_x \mathbf{e}_x + E_y \mathbf{e}_y$ as

$$W_{el} = \int_{S_{21}} \left[\sin\theta \left(\Pi + \frac{\epsilon_0 \epsilon_w}{2} E^2 \right) + \epsilon_0 \epsilon_w \times \left(-E_x^2 \sin\theta + E_x E_y \cos\theta \right) \right] dS. \quad (3)$$

One needs to obtain the electrostatic osmotic pressure Π to evaluate W_{el}. Osmotic pressure can be estimated through Poisson's equation, which states

$$\nabla \cdot \Pi = \epsilon_0 \epsilon_w (\nabla \cdot \mathbf{E}) \mathbf{E}. \quad (4)$$

Considering coordinates parallel and perpendicular to the interface, which we denote as x', y' (x' and y' are obtained by rotating the specified x-y coordinates [see Fig. 1(b)] by an angle θ in clockwise direction), and using the fact that the net electric field perpendicular to the interface is zero, i.e., $E_{y'} = 0$ (since the air-water interface is assumed to be uncharged), we can get from Eq. (4) [using the condition that when $E = 0$, $\Pi = 0$ (typically far away from the TPCL)]

$$\frac{\partial \Pi}{\partial x'} \mathbf{e}_{x'} = \frac{\epsilon_0 \epsilon_w}{2} \frac{\partial \left(E_{x'}^2 \right)}{\partial x'} \mathbf{e}_{x'} \Rightarrow \Pi = \frac{\epsilon_0 \epsilon_w}{2} E_{x'}^2 = \frac{\epsilon_0 \epsilon_w}{2} \left[E_x^2 \cos^2\theta + E_y^2 \sin^2\theta \right]. \quad (5)$$

Using Eq. (5) in Eq. (3), we get

$$W_{el} = \frac{\epsilon_0 \epsilon_w}{2} \int_{S_{21}} \left[-E_x^2 \sin^3\theta + 2 E_x E_y \cos\theta + E_y^2 (\sin^3\theta + \sin\theta) \right] dS. \quad (6)$$

C. Calculation of the electric fields E_x and E_y

To obtain W_{el}, one needs to obtain E_x and E_y along the air-liquid interface (or the plane S_{21}). To do so, we apply the model of Dörr and Hardt [27] who calculated the EDL electric field close to the TPCL in an electrolyte by approximating the domain close to the TPCL as a wedge. Here we briefly review the essential points of the calculation by Dörr and Hardt [27]. In this calculation, the dimensionless EDL electrostatic potential is $\bar{\phi} = \epsilon_0 \epsilon_w \phi / \lambda \sigma$ (where λ is the EDL thickness and σ is the charge density) and the dimensionless distances are $\bar{x} = x/\lambda$, $\bar{y} = y/\lambda$. Dörr and Hardt [27] considered the linearized Debye-Hückel treatment (requiring the assumption of weak to moderate EDL potential or charge density), so that the equation governing EDL potential distribution reads

$$\bar{\Delta} \bar{\phi} = \bar{\phi}, \quad (7)$$

where $\bar{\Delta}$ is the Laplacian in dimensionless form. The boundary conditions for the above equation are

$$\bar{\phi}|_{\bar{y} \to \infty} = 0, \quad (8)$$

$$\bar{\nabla} \bar{\phi} \cdot \mathbf{e}_x |_{\bar{x} \to \infty} = 0, \quad (9)$$

$$\bar{\nabla} \bar{\phi} \cdot \mathbf{e}_\varphi |_{\varphi = 0} = -1, \quad (10)$$

$$\bar{\nabla} \cdot \mathbf{e}_\varphi |_{\varphi = \pi - \theta} = 0. \quad (11)$$

In the above equations $\bar{\nabla}$ is the gradient operator in dimensionless form. Dörr and Hardt [27] provided a semiheuristic solution of the above sets of equations to obtain potential distribution $\bar{\phi}$ in the wedge as

$$\bar{\phi} = \exp(-\bar{y}_0), \quad (12)$$

where $\bar{y}_0 = \bar{y}_0(\bar{x}, \bar{y})$ is obtained iteratively from the equation

$$\bar{y} = \bar{y}_0 - \left[\bar{y}_0 - \frac{\bar{y}_0 - d}{c} \cos(\pi/2 - \theta) \right] \times \exp\left[-\tan(\pi/2 - \theta) \frac{c\bar{x} + (\bar{y}_0 - d)\sin(\pi/2 - \theta)}{c\bar{y}_0 - (\bar{y}_0 - d)\cos(\pi/2 - \theta)} \right], \quad (13)$$

[where $d = \ln(\frac{2\pi - 2\theta}{\pi})$ and $c = 1 + 0.36(\pi/2 - \theta)$]. Please note that eq.(13) yields $\bar{y} = \bar{y}_0$ as $\bar{x} \to \infty$.

From Eq. (13), we get

$$\frac{\partial \bar{y}_0}{\partial \bar{x}} = \frac{\tan(\pi/2 - \theta) + n_5}{1 - n_3 + n_4}, \quad (14)$$

where

$$n_3 = \exp(-m) \left[1 - \frac{\cos(\pi/2 - \theta)}{c} \right], \quad (15)$$

$$n_4 = n_1 \exp(-m) \left[\bar{y}_0 - \frac{\bar{y}_0 - d}{c} \cos(\pi/2 - \theta) \right], \quad (16)$$

$$n_5 = -n_2 \exp(-m)\left[\bar{y}_0 - \frac{\bar{y}_0 - d}{c}\cos(\pi/2-\theta)\right], \tag{17}$$

$$n_1 = \frac{\tan(\pi/2-\theta)\sin(\pi/2-\theta)}{[c\bar{y}_0 - (\bar{y}_0 - d)\cos(\pi/2-\theta)]} - \frac{\tan(\pi/2-\theta)[c - \cos(\pi/2-\theta)][c\bar{x} + (\bar{y}_0 - d)\sin(\pi/2-\theta)]}{[c\bar{y}_0 - (\bar{y}_0 - d)\cos(\pi/2-\theta)]^2}, \tag{18}$$

$$n_2 = \frac{c\,\tan(\pi/2-\theta)}{[c\bar{y}_0 - (\bar{y}_0 - d)\cos(\pi/2-\theta)]}, \tag{19}$$

$$m = \tan(\pi/2-\theta)\frac{c\bar{x} + (\bar{y}_0 - d)\sin(\pi/2-\theta)}{c\bar{y}_0 - (\bar{y}_0 - d)\cos(\pi/2-\theta)}. \tag{20}$$

Similarly, we can get

$$\frac{\partial \bar{y}_0}{\partial \bar{y}} = \frac{1+n_7}{1-n_3+n_4}, \tag{21}$$

where

$$n_7 = -n_6 \exp(-m)\left[\bar{y}_0 - \frac{\bar{y}_0 - d}{c}\cos(\pi/2-\theta)\right], \tag{22}$$

$$n_6 = \frac{c}{[c\bar{y}_0 - (\bar{y}_0 - d)\cos(\pi/2-\theta)]}. \tag{23}$$

Therefore, the electric field, in dimensionless form, can be expressed as

$$\begin{aligned}\bar{\mathbf{E}} &= \bar{E}_x\mathbf{e}_x + \bar{E}_y\mathbf{e}_y \\ &= -\frac{\partial\bar{\phi}}{\partial\bar{x}}\mathbf{e}_x - \frac{\partial\bar{\phi}}{\partial\bar{y}}\mathbf{e}_y = -\frac{d\bar{\phi}}{d\bar{y}_0}\frac{\partial\bar{y}_0}{\partial\bar{x}}\mathbf{e}_x - \frac{d\bar{\phi}}{d\bar{y}_0}\frac{\partial\bar{y}_0}{\partial\bar{y}}\mathbf{e}_y \\ &= \exp(-\bar{y}_0)\left[\frac{\tan(\pi/2-\theta)+n_5}{1-n_3+n_4}\mathbf{e}_x + \frac{1+n_7}{1-n_3+n_4}\mathbf{e}_y\right].\end{aligned} \tag{24}$$

From this dimensionless electric field, we can get the dimensional electric field as

$$\mathbf{E} = \frac{\sigma}{\epsilon_0\epsilon_w}\bar{\mathbf{E}} = \frac{\sigma}{\epsilon_0\epsilon_w}[\bar{E}_x\mathbf{e}_x + \bar{E}_y\mathbf{e}_y] = E_x\mathbf{e}_x + E_y\mathbf{e}_y, \tag{25}$$

where

$$\begin{aligned}E_x &= \frac{\sigma}{\epsilon_0\epsilon_w}\exp(-\bar{y}_0)\left[\frac{\tan(\pi/2-\theta)+n_5}{1-n_3+n_4}\right], \\ E_y &= \frac{\sigma}{\epsilon_0\epsilon_w}\exp(-\bar{y}_0)\left[\frac{1+n_7}{1-n_3+n_4}\right].\end{aligned} \tag{26}$$

III. RESULTS

In this section, we first present the results expressing the variation of the dimensionless EDL potential and electric field as a function of the wedge angle. These results are relevant for the contact angle on any surface as long as the approximations (see Sec. I) are valid. Application of these electric field variations to obtain the contact angle change becomes possible only when one can pinpoint the corresponding EDL thickness (function of the ion concentration) and the surface charge density. Here, we shall provide results for two surfaces (bare silica and OTS-silicon), where these two parameters are interrelated as a function of the ion concentration and buffer *p*H. The choice of these two substrates is motivated by the abundance of information on their dissociation chemistry (providing a well-established interrelationship between the surface charge density and the EDL thickness) and their relevance in the context of nanobubble formation.

A. Variation of the EDL potential and electric fields in the wedge geometry

Figure 2 shows the variation of the dimensionless EDL electrostatic potential along the air-water interface (of the bubble or the drop). We show the results as a function of the dimensionless transverse coordinate $\bar{y}$, which automatically fixes the corresponding axial coordinate $\bar{x}$, since along the air-water interface, $\bar{y}$ and $\bar{x}$ are connected as $\bar{x} = \bar{y}/\tan(\pi/2-\theta)$. We find an intuitive result in the sense that we notice a progressive decrease in the EDL potential away from the TPCL (charge on the interface is localized at the TPCL, since the solid-liquid interface is charged). A very similar result was obtained by Dörr and Hardt [27]. On the other hand, we obtain a relatively more involved result when we find that for larger θ (or smaller wedge angle, given by $\pi - \theta$), the potential at the air-water interface is larger at locations close to the TPCL (characterized by smaller values of $\bar{y}$), but at locations substantially away from the TPCL there is not much effect of the wedge angle on the EDL potential.

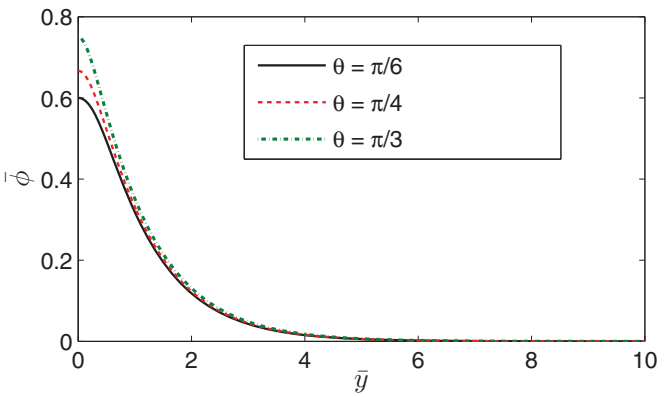

FIG. 2. (Color online) Variation of the dimensionless EDL electrostatic potential along the air-water interface (of the bubble or the drop) for different values of the contact angle. We show the result as a function of the dimensionless transverse coordinates $\bar{y}$, whereas the corresponding axial coordinates $\bar{x}$ are defined as $\bar{x} = \bar{y}/\tan(\pi/2-\theta)$.

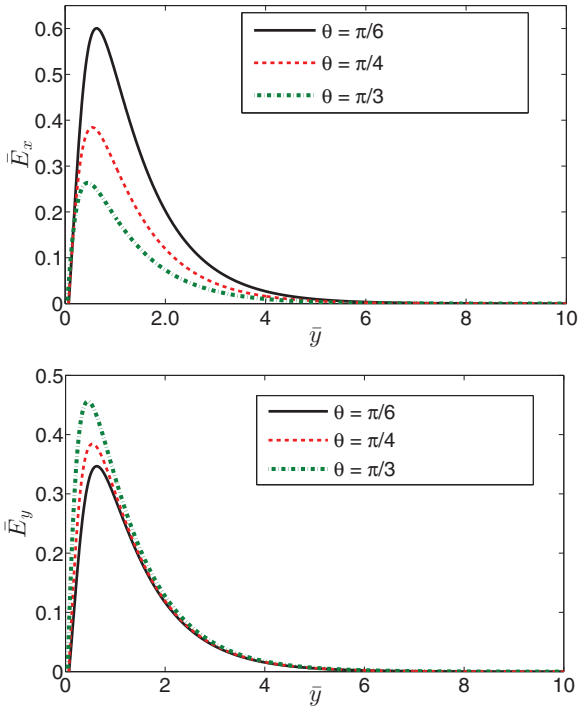

FIG. 3. (Color online) Variation of the dimensionless (a) axial electric field and (b) transverse electric field along the air-water interface for different values of the nanobubble contact angle. We show the result as a function of the dimensionless transverse coordinates $\bar{y}$, whereas the corresponding axial coordinates $\bar{x} = \bar{y}/\tan(\pi/2 - \theta)$.

Figures 3(a) and 3(b) show the variation of the axial and the transverse electric fields at the air-water interface. Quite remarkably, at locations very close to the TPCL both components of the electric field are negligible—such behavior can be justified by a close to uniform value of the EDL electrostatic potential at such spatial locations (see Fig. 2). These results are extremely nonintuitive in case one compares them with the electric field inside an EDL near an ordinary charged surface, where one invariably finds an increase in the EDL electric field at locations close to the charged surface. As one moves away from the TPCL, however, the EDL potential shows finite spatial variation (see Fig. 2), causing both $\bar{E}_x$ and $\bar{E}_y$ to increase with $\bar{y}$ for small (<1) values of $\bar{y}$. Please note that this increase in the electric fields occurs (for $\bar{y} < \bar{y}_c$) despite the fact that the corresponding EDL potential is lowered with increase in $\bar{y}$ (for $\bar{y} < \bar{y}_c$), and can be attributed solely to the corresponding increase in the EDL potential gradient (despite lowering EDL potential). However, for $\bar{y} > \bar{y}_c$, the consequence of monotonic decrease of the EDL potential becomes crucial, leading to a monotonic lowering of the EDL electric field. Finally, quite intuitively, the decrease in the wedge angle leads to an enhanced (reduced) influence of the transverse (axial) electric fields, with the two (transverse and axial electric fields) becoming equal for $\theta = \pi/4$. Therefore, Figs. 3(a) and 3(b) provide unique examples of nonmonotonic spatial variation of EDL electric fields away from a charged interface, and can be attributed to the unique wedge configuration of the system.

B. Variation of the contact angle

Figures 2 and 3 provide the dimensionless spatial variation of the electrostatic potential and fields at the wedge, representing the TPCL. In order to obtain the effect of EDL electrostatics at the wedge in altering the drop or bubble contact angle, we need to know the dimensional magnitude of these electric fields, which will give the corresponding dimensional values of $W_{el}(\theta)$. For that purpose, values of the charge density σ and the EDL thickness λ are essential. However, these two variables are not independent; rather they are connected by the chemical equilibrium dynamics of the electrolyte-charged-solid interface. For the present study, we consider two surfaces, namely, bare silica and OTS-silicon. OTS-silicon substrates are prepared by applying a molecular coating of OTS on the bare silica, and the surface is characterized by a bare charge density $f\sigma$, where σ is the charge density of bare silica surface and f is a fraction (lower than unity), which is smaller for a greater coverage of OTS [58]. Motivation to consider bare silica surface is twofold: First is the massive use of bare silica or silanized surfaces (which are some derivative of the bare silica surface) in studying the EDL structure and its consequence in micro-nanoscale transport [58,59], and second is the availability of knowledge of the chemical equilibrium dynamics of bare silica [28,29]. Similarly, OTS-silicon surface is extremely popular in studying the origin and dynamics of surface nanobubbles [52,60,61]. Therefore, by studying the wedge-structure EDL-mediated alterations of the contact angle for these two surfaces, we ensure that our analysis provides results that are relevant to the general problem of drop or bubble contact angles, as well as the specific problem of surface nanobubbles.

The chemical equilibrium reactions for both bare silica and OTS-silicon surfaces have been studied extensively [15,28,29,59]. We refrain from providing the detailed derivations, for which we request the reader to kindly see the Appendix of our previous paper [15]. The key outputs of the analysis [15] are the charge density and the zeta potential, and the input parameters are the buffer pH, ionic concentration, and fractional coverage f (for the OTS-silicon surface). These are tabulated below.

Figure 4 shows the variation in the change of the contact angle $\Delta\theta = \theta_0 - \theta$ with original (EDL-independent) contact

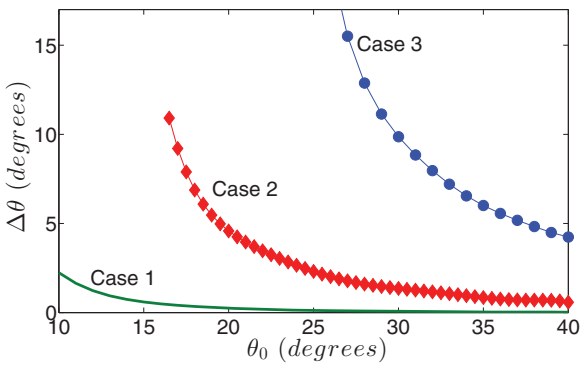

FIG. 4. (Color online) Variation of change in the nanobubble contact angle $\Delta\theta = \theta_0 - \theta$ for bare silica surface with the original (EDL-independent) contact angle θ_0 for three different cases, which are case 1: pH = 5, c = 1 M, case 2: pH = 6, c = 1 M, and case 3: pH = 7, c = 1 M (corresponding σ and ζ values are provided in Table I).

TABLE I. Bare silica surface charge density (σ) and zeta potential (ζ) as a function of buffer pH and ion concentration (c). EDL thickness λ is connected to c as $\lambda = (\epsilon_0\epsilon_w k_B T/2000 N_A c e^2 z^2)^{1/2}$.

pH	c (M)	λ (nm)	σ (mC/m^2)	ζ (mV)
5	1	0.33	−16.6	−4.2
	0.1	1	−8.9	−11.11
	0.01	3.33	−5.5	−23.2
6	1	0.33	−69.75	−13.33
	0.1	1	−30.6	−31.8
7	1	0.33	−174.6	−22.8
	0.1	1	−81.3	−54.6
8	1	0.33	−314.4	−29.3
	0.1	1	−181	−70.4
9	1	0.33	−466.8	−33.7

angle θ_0 for the bare silica surface. We consider different combinations of buffer pH and ion concentration values (yielding different values of ζ and σ; see caption of Fig. 4). For a given ionic concentration, increase in pH increases ζ and σ values for the bare silica surface, as has been well reported in the literature [28,29]. This increase would necessarily mean an increase in hydrophilicity inducing tendency of the EDL effects, as is reflected in Fig 4. Further, for a given pH and ionic concentration, $\Delta\theta$ is more for smaller θ_0—this can be interpreted from a larger influence of the axial electric field for smaller θ_0 [see Fig. 3(a)]. Please note that for higher pH values (e.g., pH = 6,7), one cannot get a finite $\Delta\theta$ for small enough θ_0, since for such cases one may have $\Delta\theta > \theta_0$—this will signify a situation where a stable drop or a bubble cannot be formed. Also, we provide results for only those pH and c values for which the resultant electrostatic potential scale ($\sim\sigma\lambda/\epsilon_0\epsilon_r$) is small enough for the application of the Debye-Hückel linearization approach (see Table I).

Figure 5 shows the variation in $\Delta\theta$ as a function of θ_0 for different values of fractional surface coverage of OTS (larger

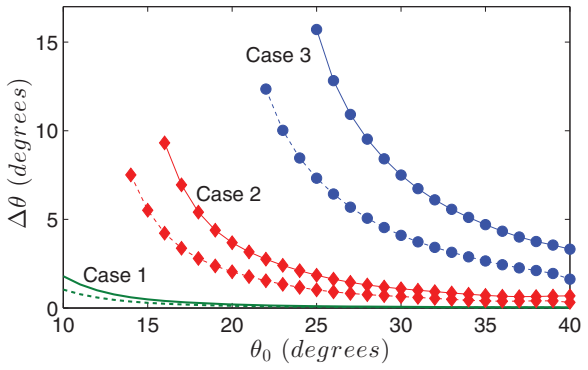

FIG. 5. (Color online) Variation of change in the nanobubble contact angle $\Delta\theta = \theta_0 - \theta$ for OTS-silica surface with the original (EDL-independent) contact angle θ_0 for three different cases, which are case 1: pH = 5, c = 1 M, case 2: pH = 6, c = 1 M, and case 3: pH = 7, c = 1 M (corresponding σ and ζ values are tabulated in Table I). For each of these cases, we consider two different values of fractional OTS coverage, namely, $f = 0.9$ (plot shown by a bold line) and $f = 0.7$ (plot shown by a dashed line).

TABLE II. OTS-silicon surface charge density (σ) and zeta potential (ζ) as a function of buffer pH, ion concentration (c), and fractional surface coverage of OTS (f).

pH	c (M)	λ (nm)	f	σ (mC/m^2)	ζ (mV)
5	1	0.33	0.9	−14.94	−4.3
	1	0.33	0.7	−11.62	−4.4
6	1	0.33	0.9	−62.78	−14.4
	1	0.33	0.7	−48.83	−14.6
7	1	0.33	0.9	−157.14	−24.3
	1	0.33	0.7	−122.2	−25.6
8	1	0.33	0.9	−282.96	−31.0
	1	0.33	0.7	−220.08	−32.1

coverage implies smaller f). Results (Table II, Fig. 5) indicate a lowering in $\Delta\theta$ with an increase in surface coverage (or smaller f). Other effects, such as more pronounced values of $\Delta\theta$ for larger pH and smaller θ_0, or a lack of finite $\Delta\theta$ for smaller θ_0 and larger pH are equally prevalent for this case too.

IV. DISCUSSIONS

The model for the wedge-geometry-based EDL-induced variation of the contact angle is valid for any system where there is a drop or a bubble formation in the presence of electrolyte ions. In fact, the model can even be employed for formation of a drop in an immiscible liquid, as long as the liquid-liquid interface is uncharged and one of the liquids can sustain an EDL. Of course the dimensionless variation in the electric field and the electrostatic potential predicted by our model (see Figs. 2 and 3) are valid for any combination of solid-liquid and liquid-air interfaces. However, for exact quantification of the change in the contact angle we need to specify the surface and the corresponding interrelationship (if any) between the parameters such as pH, EDL thickness, zeta potential, and surface charge density. Given the surge in recent interests in understanding the effect of electrolyte ions in applications that involve contact line dynamics on charged surfaces, e.g., electrowetting [62–64], wetting of inhomogeneous surfaces [16], etc., this model will ensure a hitherto missing correct accounting of the EDL effect in contact angle variations.

As has been discussed previously, the main motivation of this study, which of course has a much more general validity, has been in understanding the effect of added salt in the morphology of preformed surface nanobubbles. There have been two schools of thought regarding the impact of added salt on the morphology of the preformed surface nanobubbles. The first view, mostly based on the evidence obtained from experiments [60,65], inferred that added salt will have no influence on the morphology of preformed surface nanobubbles. The experiments were carried out on HOPG (highly ordered pyrolytic graphite) for moderate and large salt concentrations [60,65] as well as on OTS-silicon substrates (there is no specification of what has been the pH and ionic concentration values corresponding to which surface nanobubbles were studied on OTS-silicon substrates) [60]. Through a

detailed scaling argument, we introduced a second view to this problem, where we demonstrated that for substantially alkaline solutions and for extreme (very large or very small) values of the salt concentrations, preformed surface nanobubbles on OTS-silicon may demonstrate significant variation of the contact angle [15]. Our idea was based on the fact that for the stated conditions, the ionization of the bare silica leads to a substantially large zeta potential (∼0.2–0.3 V) ensuring an equivalently large electrostatic wetting tension, thereby leading to the noticeable alteration in the nanobubble contact angle. The other implicit requirement of our previous model was that there would be minimal coverage of the silica surface by OTS, else the corresponding lowering of the zeta potential would be large enough to ensure that the nanobubble contact angle shows negligible reduction. However, less coverage of OTS would mean lesser coverage of the nanobubbles, which is not always a desirable condition. In the present calculation, we improve these understandings. Our analytical model establishes that even for extremely moderate (weakly acidic or neutral) values of buffer *p*H, we should witness a substantially large deviation in the nanobubble contact angle formed on an OTS-silicon surface. One can also understand from our present analysis why there is no report on the effect of added salt for nanobubbles on OTS-silicon (e.g., in the study of Zhang *et al*. [60]). On an OTS-silicon surface, salt-independent nanobubble contact angle (θ_0) is around 12° [60], so there is a likelihood that on salt addition the bubbles will actually disappear (since $\Delta\theta \geqslant \theta_0$, as has been discussed in Fig. 5).

Finally, we discuss the recovery of experimental results with our theory. Experimental studies that give the role of added salt on contact angle variation are plentiful [64,66–69]. However, what is substantially missing are those studies that provide contact angle variation for surfaces with a known connection between ζ, σ, and λ (e.g., surfaces such as bare silica or OTS-silicon)—without such connection one cannot validate our proposed theory with experimental results. There is only a handful of studies that provide experimental results on contact angle variation on such surfaces [70]; but the problem is the contact angle values vary massively depending on the method employed to calculate them [70]. In the context of effect of added salt on preformed surface nanobubbles, for surface nanobubbles formed on a HOPG surface there is hardly any effect [60,65], whereas for the nanobubbles formed on an OTS-silicon surface, there is no report of the existence of surface nanobubbles in the presence of added salt [60]. This may be an implicit validation of our theory, as explained above.

V. CONCLUSIONS

In this paper, based on a wedgelike assumption of the region around the TPCL, we provide a detailed analytical solution for the effect of added salt (and resulting EDL) in altering the contact angle of drops or bubbles in an electrolytic environment. We provide results for sample substrates, such as bare silica or OTS-silicon, and demonstrate that for moderate *p*H and large ionic concentrations the impact of the EDL interactions may lead to large lowering of contact angles, or may even enforce a disappearance of a drop or a bubble. Although the model can predict the EDL effects in any problem of contact angle, we discuss a special case of the impact of added salt on preformed surface nanobubbles, and establish, unlike previous experimental [60,65] or theoretical studies [15], that the effect of added salt in causing a substantial, measurable variation in nanobubble morphology is ubiquitous and universal even for most moderate conditions.

ACKNOWLEDGMENT

The authors gratefully acknowledge the Natural Sciences and Engineering Research Council of Canada (NSERC) for providing financial support to S.D. in the form of the Banting Postdoctoral Fellowship.

[1] P.-G. de Gennes, F. Brochart-Wyart, and D. Quéré, *Capillarity and Wetting Phenomena: Drops, Bubbles, Pearls, Waves* (Springer, New York, 2003).
[2] P.-G. de Gennes, Rev. Mod. Phys. **57**, 827 (1985).
[3] L. Leger and J.-F. Joanny, Rep. Prog. Phys. **55**, 431 (1992).
[4] A. Oron, S. H. Davis, and S. G. Bankoff, Rev. Mod. Phys. **69**, 931 (1997).
[5] V. M. Starov, M. G. Velarde, and C. J. Radke, *Wettability* (CRC, Boca Raton, 2007).
[6] D. Bonn, J. Eggers, J. Indekeu, J. Meunier, and E. Rolley, Rev. Mod. Phys. **81**, 739 (2009).
[7] J. H. Snoeijer and B. Andreotti, Annu. Rev. Fluid Mech. **45**, 269 (2013).
[8] P. Roach, N. J. Shirtcliffe, and M. I. Newton, Soft Matter **4**, 224 (2008).
[9] B. Bhushan, Y. C. Jung, and K. Koch, Philos. Trans. R. Soc., A **367**, 1631 (2009).
[10] D. Quéré, Annu. Rev. Mater. Res. **38**, 71 (2008).
[11] K. Liu and L. Jiang, Annu. Rev. Mater. Res. **42**, 231 (2012).
[12] P. R. Waghmare, S. Das, and S. K. Mitra, Sci. Rep. **3**, 1862 (2013).
[13] F. Mugele and J.-C. Baret, J. Phys.: Condens. Matter **17**, R705 (2005).
[14] W. C. Nelson and C.-J. 'CJ' Kim, J. Adhesion Sci. Technol. **26**, 1747 (2012).
[15] S. Das, Phys. Rev. E **84**, 036303 (2011).
[16] S. Das, S. K. Mitra, and S. Chakraborty, Phys. Rev. E **86**, 011603 (2012).
[17] K. Kang, I. Kang, and C. Lee, Langmuir **19**, 5407 (2003).
[18] K. Kang, I. Kang, and C. Lee, Langmuir **19**, 6881 (2003).
[19] K. Kang, I. Kang, and C. Lee, Langmuir **19**, 9334 (2003).
[20] K. Kang and I. Kang, Langmuir **19**, 9962 (2003).
[21] C. K. Hua, I. S. Kang, K. H. Kang, and H. A. Stone, Phys. Rev. E **81**, 036314 (2010).
[22] S. Das, S. Chakraborty, and S. K. Mitra, Phys. Rev. E **85**, 046311 (2012).
[23] S. Das, S. K. Mitra, and S. Chakraborty, Phys. Rev. E **86**, 056317 (2012).

[24] R. J. Hunter, *Zeta Potential in Colloid Science* (Academic, London, 1981).
[25] D. C. Grahame, Chem. Rev. **41**, 441 (1947).
[26] H.-F. Kuo, D.-H. Lien, and W.-K. Hsu, Appl. Phys. Lett. **89**, 044109 (2006).
[27] A. Dörr and S. Hardt, Phys. Rev. E **86**, 022601 (2012).
[28] S. Behrens and D. Grier, J. Chem. Phys. **115**, 6716 (2001).
[29] M. Wang and A. Revil, J. Colloid Interface Sci. **343**, 381 (2010).
[30] C. Wagner, Z. Phys. **25**, 474 (1924).
[31] L. Onsager and N. N. T. Samaras, J. Chem. Phys. **2**, 528 (1934).
[32] E. C. Mbamala and H. H. von Grünberg, J. Phys. Condens. Matter **14**, 4881 (2002).
[33] W. A. Weyl, J. Colloid Sci. **6**, 389 (1951).
[34] R. J. Good, J. Phys. Chem. **61**, 810 (1957).
[35] A. Frumkin, Electrochim. Acta **2**, 351 (1960).
[36] J. R. Farrel and P. J. McTigue, J. Electroanal. Chem. **139**, 37 (1982).
[37] M. Hampton and A. V. Nguyen, Adv. Colloid Interface Sci. **154**, 30 (2010).
[38] V. Craig, Soft Matt. **7**, 40 (2011).
[39] J. R. T. Seddon and D. Lohse, J. Phys.: Condens. Matter **23**, 133001 (2011).
[40] J. R. T. Seddon, D. Lohse, W. A. Ducker, and V. S. J. Craig, Chem. Phys. Chem. **13**, 2179 (2012).
[41] J. W. G. Tyrrell and P. Attard, Phys. Rev. Lett. **87**, 176104 (2001).
[42] M. Switkes and J. W. Ruberti, Appl. Phys. Lett. **84**, 4759 (2004).
[43] X. H. Zhang, A. Quinn, and W. A. Ducker, Langmuir **24**, 4756 (2008).
[44] G. Liu, Z. Wu, and V. S. J. Craig, J. Phys. Chem. C **112**, 16748 (2008).
[45] S. Karpitschka, E. Dietrich, J. R. T. Seddon, H. J. W. Zandvliet, D. Lohse, and H. Riegler, Phys. Rev. Lett. **109**, 066102 (2012).
[46] E. R. White, M. Mecklenburg, S. B. Singer, S. Aloni, and B. C. Regan, Appl. Phys. Express **4**, 055201 (2011).
[47] C. U. Chan and C-D. Ohl, Phys. Rev. Lett. **109**, 174501 (2012).
[48] P. Attard, M. P. Moody, and J. W. G. Tyrrell, Physica A **314**, 696 (2002).
[49] S. M. Dammer and D. Lohse, Phys. Rev. Lett. **96**, 206101 (2006).
[50] B. M. Borkent, S. M. Dammer, H. Schönherr, G. J. Vancso, and D. Lohse, Phys. Rev. Lett. **98**, 204502 (2007).
[51] M. P. Brenner and D. Lohse, Phys. Rev. Lett. **101**, 214505 (2008).
[52] W. A. Ducker, Langmuir **25**, 8907 (2009).
[53] J. R. T. Seddon, E. S. Kooij, B. Poelsema, H. J. W. Zandvliet, and D. Lohse, Phys. Rev. Lett. **106**, 056101 (2011).
[54] J. R. T. Seddon, H. J. W. Zandvliet, and D. Lohse, Phys. Rev. Lett. **107**, 116101 (2011).
[55] S. Das, J. H. Snoeijer, and D. Lohse, Phys. Rev. E **82**, 056310 (2010).
[56] S. Das, Phys. Rev. E **83**, 066315 (2011).
[57] J. H. Weijs, J. H. Snoeijer, and D. Lohse, Phys. Rev. Lett. **108**, 104501 (2012).
[58] D. Stein, M. Kruithof, and C. Dekker, Phys. Rev. Lett. **93**, 035901 (2004).
[59] S. Das, K. Subramanian, and S. Chakraborty, Colls Surf., B **58**, 203 (2007).
[60] X. Zhang, N. Maeda, and V. Craig, Langmuir **22**, 5025 (2006).
[61] N. Ishida, T. Inoue, M. Miyahara, and K. Higashitani, Langmuir **16**, 6377 (2000).
[62] C. W. Monroe, L. I. Daikhin, M. Urbakh, and A. A. Kornyshev, Phys. Rev. Lett. **97**, 136102 (2006).
[63] M. Paneru, C. Priest, R. Sedev, and J. Ralston, J. Phys. Chem. C **114**, 8383 (2010).
[64] C. P. Lee, B. Y. Fang, and Z. H. Wei, Analyst **138**, 2372 (2013).
[65] M. Hampton and A. Nguyen, Miner. Eng. **22**, 786 (2009).
[66] P. B. Welzel, C. Rauwolf, O. Yudin, and K. Grundke, J. Colloid Interface Sci. **251**, 101 (2002).
[67] R. Ghosh Chaudhuri and S. Paria, J. Colloid Interface Sci. **337**, 555 (2009).
[68] K. B. Borisenko, E. A. Evangelou, Q. Zhao, and E. W. Abel, J. Colloid Interface Sci. **326**, 329 (2008).
[69] A. Lundblad and B. Bergman, J. Electrochem. Soc. **144**, 984 (1997).
[70] J. Lützenkirchen, C. Richter, and F. Brandenstein, Adsorption **16**, 249 (2010).